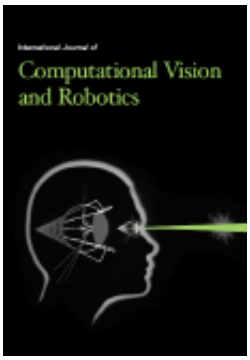

International Journal of Computational Vision and Robotics

ISSN online: 1752-914X - ISSN print: 1752-9131
https://www.inderscience.com/ijcvr

Obstacle detection technique to solve poor texture appearance of the obstacle by categorising image's region using cues from expansion of feature points for small UAV

Muhammad Faiz Ramli, Syariful Syafiq Shamsudin

DOI: 10.1504/IJCVR.2022.10044362

Article History:

Received:	19 May 2021
Accepted:	20 December 2021
Published online:	30 November 2022

Obstacle detection technique to solve poor texture appearance of the obstacle by categorising image's region using cues from expansion of feature points for small UAV

Muhammad Faiz Ramli and
Syariful Syafiq Shamsudin*

Department of Aeronautical Engineering,
Universiti Tun Hussein Onn Malaysia,
86400, Parit Raja, Johor, Malaysia
Email: faizr@uthm.edu.my
Email: syafiq@uthm.edu.my
*Corresponding author

Abstract: Achieving a reliable obstacle detection system for small unmanned aerial vehicle (UAV) is very challenging due to its size and weight constraints. Prior works tend to employ the vision sensor as main detection sensor but resulting to high dependency on texture appearance while not having distance sensing capabilities. Besides, most of wide spectrum range sensors are heavy and expensive. The contribution of this work is on different based-sensor integration technique to increase reliability of detection. A method was developed to create trusted avoidance path by categorising the region in environment into two regions, which are the obstacle region and free region. Cues from expansion of the features points are used to extract the depth information of the environment and classify the region in the image frame. The results show that the proposed system able to handle multiple obstacle and create safe path regardless of the texture and size of the obstacle.

Keywords: obstacle detection; feature points; region classification; safe avoidance path; vision-based-sensor; range-based-sensor; speeded up robust features; SURF; convex hull; depth perception.

Reference to this paper should be made as follows: Ramli, M.F. and Shamsudin, S.S. (2023) 'Obstacle detection technique to solve poor texture appearance of the obstacle by categorising image's region using cues from expansion of feature points for small UAV', *Int. J. Computational Vision and Robotics*, Vol. 13, No. 1, pp.91–115.

Biographical notes: Muhammad Faiz Ramli received his degree in Aircraft Engineering Technology from the Malaysia Institute of Aviation Technology. He pursued his Master's in Aerospace Mechanics and Avionics from the Institut supérieur de l'aéronautique et de l'espace. He completed his Doctorate Philosophy in Mechanical Engineering specialising in UAV System. Currently, he is working as a researcher and Lecturer in the Department of Aeronautical Engineering, Universiti Tun Hussein Onn Malaysia. His research interests are in UAV system and computer vision.

Syariful Syafiq Shamsudin received his BEng in Mechanical-Aeronautics from the Universiti Teknologi Malaysia, Skudai, Malaysia, in 2003, MEng in Mechanical Engineering from Universiti Teknologi Malaysia, Skudai,

Malaysia, in 2007, and PhD in Mechanical Engineering from University of Canterbury, Christchurch, New Zealand, in 2013. He is currently a Senior Lecturer with the Department of Aeronautical Engineering, Faculty of Mechanical and Manufacturing Engineering, Universiti Tun Hussein Onn Malaysia. His current research interests include aircraft and rotorcraft system identification, intelligent adaptive control and unmanned aerial system design.

1 Introduction

Hypothetically, the unmanned aerial vehicle (UAV) platform has great potential to perform numerous tasks such as monitoring the environment (Torrero et al., 2014), massive building and structure inspection (Deng et al., 2014; Eschmann et al., 2012), search and rescue activities (Scherer et al., 2015; Rudol and Doherty, 2008; Erdos et al., 2013) and others. Most of these tasks require the UAV to achieve a higher level of autonomy in its embedded system. One of the tasks in the autonomous system for the UAV is the operation to identify the appearance of any obstacles that are being introduced to the UAV and ultimately create a manoeuvre action plan. The obstacle detection and avoidance operation can be very challenging to the UAV platform, especially for a small-sized UAV. This is due to the payload capacity and physical size constraints of the UAV. Typically, the obstacle detection system for UAV depends on the type of sensors being installed onboard the UAV, which is either vision-based sensors or range-based sensors. Selecting the proper sensors to be placed onboard the UAV plays a critical role in the system operation, where each of the aforementioned techniques has its own advantages and disadvantages. For example, the vision-based sensor method can provide rich information regarding the bearing of the detected obstacles in the operating environment. However, the distance from the UAV to obstacles are poorly recognised and estimated. Besides, the detection will heavily rely on the texture appearance of the obstacle. Conversely, range-based sensor is excellent in determining the distance value of the detected obstacle, but there is a lack of information about the location of the detected obstacle in the surrounding environment.

Since most of the commercial UAVs at present are small in size, the development of the obstacle detection system becomes more complicated due to the mentioned constraints. As a result, the researchers need to find a balanced line between the performance of the system and the constraints by the UAV platform. UAV needs a robust obstacle detection system that can determine trusted safe path avoidance regardless of texture appearance, obstacles sizes and number of obstacles introduced in the environment. On top of that, the system must perceive a robust distance value to obstacles, so that, warning for collision and decision for avoidance can be made. Although it may be possible for a larger UAV, it is still difficult for small UAV to achieve. Therefore, in this paper, we present a method to meet these needs and enhance the detection capability by integrating multi-sensors which are camera sensor and simple light detection and ranging (LIDAR) sensors into the system. We use LIDAR as initial detection in term of detecting distances and queue for activating the camera. To approximate the obstacle region, free space region and detect the safe avoidance path, we use object size changes and distance relation with respect to an image using feature detection of speeded up robust features (SURF) algorithm.

The focus of the research can be observed through these questions: first, would it be possible to integrate the range-based sensor and vision-based sensor together into one detection system to enhance the performance of the detection for small-sized UAV? Secondly, what would be the solution for the vision-based sensor detection to detect and recognise the appearance of the poor textured obstacle or texture-less obstacle in the environment? Thirdly, how to create the reliable safe avoidance path without using any tolerance extension from the detected obstacle? Finally, how to expand the horizon of the previous vision-based obstacle detection system to face with the environment which contains multiple obstacles that can also have many configurations (e.g., distance, texture appearance, and size)? The rest of the paper is organised as follows: Section 2 introduces the related works that are associated with obstacle detection technique for UAV. The framework of the proposed obstacle detection system is described in Section 3. Section 4 presents the implementation and experiment setup to evaluate the proposed system. Results are presented and discussed in Section 5. Finally, Section 6 is dedicated to the conclusions and future works of the work.

2 Related works

Constraints that are mentioned above are the ultimate factors for the researcher to choose the vision-based sensor as the source of the environmental information for the obstacle detection operation. Most commercial UAVs are already equipped with the vision-based sensor, which is the monocular camera sensor. By using the proper vision algorithms, the appearance of the obstacle in the operating environment can be detected (Payal et al., 2020). For example, Zufferey and Floreano (2006) and Yoo et al. (2011) have employed the optical flow method produced by the image frames sequence to avoid any obstacle that can pose a catastrophic to the UAV platform. However, this method is only reliable and effective for centring the UAV in the operating environment. Besides, the optical flow method has poor ability in detecting the appearance of the frontal obstacle (Al-Kaff et al., 2017; Al-Kaff, 2017).

Nhair and Al-Assadi (2020) uses edge detection to detect the free zones in flying environment. However, this method will be less reliable if the environment is fully textured. Another example is the feature size expansion (Al-Kaff et al., 2017; She et al., 2021). This method suffers from creating a trusted safe avoidance path after encountering the detected obstacle in the operating environment. It is unable to detect the free region available from the observed operating environment, whereby the safe avoidance path is thus assumed by the tolerance extension from the detected obstacle feature points. As a consequence, the path for the avoidance manoeuvre is not reliable considering any encountered obstacles will have random textures and features.

In most cases, the vision algorithms available will depend a lot on the texture of the obstacles; if the obstacle surface is texture-less, it will not be able to execute the detection process. Moreover, previous vision obstacle detection and avoidance systems only focus on the detection of the obstacle that is situated ahead and directly in front of the UAV (Mori and Scherer, 2013; Al-Kaff, 2017; Aguilar et al., 2017). In relation to that, the UAV will be exposed to collision risk during mission operation considering the vision sensor does not contain any distance sensing capabilities. Considering that the vision-based obstacle detection system will highly depends on the computation of the

vision algorithm in each consecutive captured image frames, the possibility to have latency on the computation in real time will be high (Leong et al., 2021). In addition, the judgement towards the obstacle with respect to its estimated distance and bearing will also be negatively affected (real time effect). In order to work with depth estimation of the environment, researchers tend to employ the stereo vision sensor to relatively estimate the distance of the observed environment from the UAV, which includes the obstacles (Carrio et al., 2020; Majumder et al., 2015). However, the major problem for the stereo vision sensor is the length constraints of the baseline for both of the attached camera sensors, which in turn can decrease the accuracy of the estimation. In addition, the weight and size of the camera are also considered as problems for the stereo vision sensor system.

Apart from the vision-based sensor, the range-based sensor (Whalley et al., 2009; Kim et al., 2014; Bachrach et al., 2009) has also been explored by the researchers to be used in the obstacle detection system. Although the range-based sensor is very reliable in detecting the appearance of the obstacles and building the depth estimation of the environment, most of the reliable range-based sensors (e.g., SICK, Hokuyo, Velodyne Puck, etc.) are heavy, massive, and very expensive to be practically used in a small-sized commercial UAV. Table 1 summarise the problems or hurdles of related works

Table 1 Summary of related works

Related works method	*Hurdle*
Optical flow	Only reliable for centring the UAV and poor ability in detecting the frontal obstacle.
Edge detection (segmentation)	Less reliable if the environment is heavily textured.
Feature size expansion	Suffer from creating trusted safe avoidance path. It also unable to identify the available free region from the environment. This method will depend on the texture appearance of the obstacle and it only focused on the detection of the frontal obstacle.
Stereo vision	Length constraints of the baseline for both of the attached camera sensors. In addition, weight and size of the camera are also considered as challenging aspect.
Range sensor	Most of the reliable range-based sensors are heavy, massive and expensive.
Perspective (Bills et al., 2011)	Limited to indoor environment.
Texture variation (De Croon et al., 2011)	Difficulty when dealing with high textured environment.

Our approach uses integration of different-based-sensor to enhance the capability of the detection system when compared to single sensor obstacle detection system. Our work categorising the region in the image frame into obstacle region and free region to obtain the ultimate safe avoidance path for UAV. This effort also takes into account the nature of the obstacle in the environment which includes the distance on the obstacle, multiple introduced obstacle, position, texture appearance and UAV configuration.

Figure 1 Framework of the proposed obstacle detection system (see online version for colours)

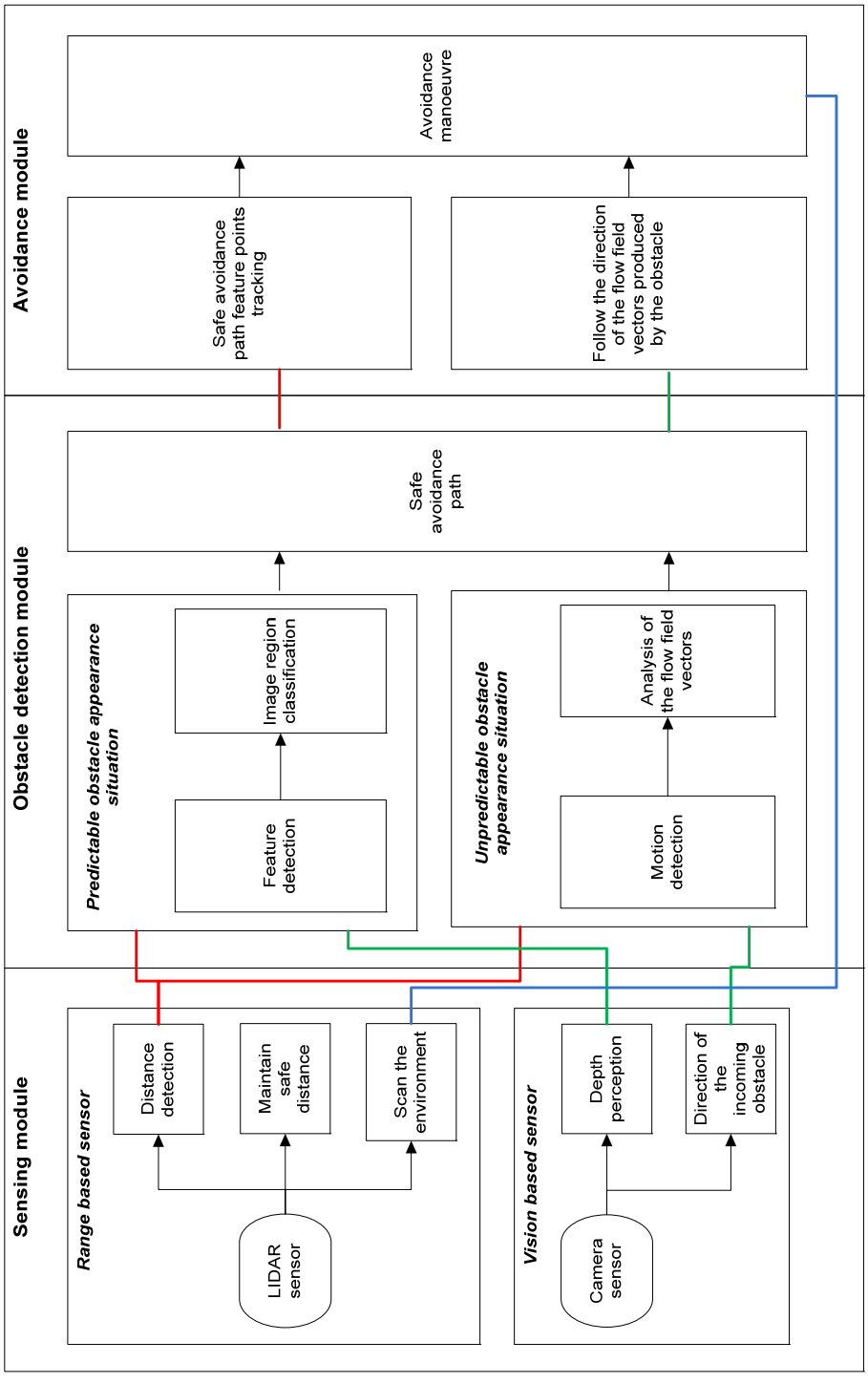

3 Proposed obstacle detection system framework

The framework of the proposed system contains three modules, which are the sensing module, obstacle detection module, and avoidance module as illustrated in Figure 1. In sensing module, there are two sensors used in the system which are LIDAR and monocular camera sensor. Apart from detecting the distance of the obstacle from the UAV platform, the LIDAR sensor will also acts as the safety device for the proposed obstacle detection system by maintaining the safe distance from any objects. In addition, the capability of the LIDAR sensor to scan the environment is needed during the avoidance manoeuvre to ensure the safety of the avoidance path. The distance detection procedure will be applied to both situations which are predictable and unpredictable obstacle appearance situations. In this paper, only predictable obstacle appearance situation is discussed (obstacle detection module).

For the vision-based sensor, the image frames captured by the camera sensor are used to derive the depth perception of the environment, so that, the distance pertaining to the surrounding environment can be observed. In obstacle detection module, image region classification technique is developed based on the detection of the feature points in the captured image frames. This region classification technique is developed to categorised the surrounding environment into obstacle region and free safe region. After the free regions in the image frame are identified, these regions are further refined by image processing to produce the path for safe avoidance known as the safe avoidance path. Finally, once the safe avoidance path is identified, the avoidance manoeuvre will be executed.

Figure 2 Series of distance detection and image frames captured by the camera sensor (see online version for colours)

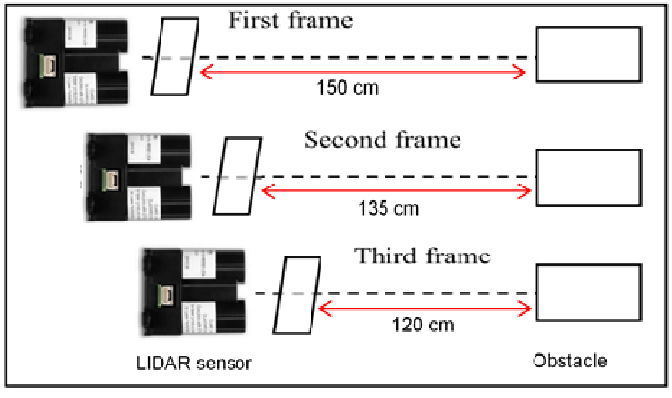

3.1 Distance detection

The main purpose of the range sensor in the proposed system is to provide an accurate distance value to the proposed system and trigger the vision sensor to initiate the detection process further. Furthermore, the range sensor can function as a safety device or guidance for the proposed system when the UAV is flying through the safe avoidance path region. There are three distance series that are needed to be detected by the LIDAR sensor and these distance values are related to the obstacle views from the image frames.

The selected threshold values for the three distance series mentioned are 150 cm, 135 cm and 120 cm. As seen in Figure 2, each of the distance values (image frames) are separated apart by 15 cm. When all of the three image frames have been captured, the proposed system will instruct the LIDAR sensor to change from active into passive mode until the avoidance manoeuvre is ready to be executed.

3.2 Depth perception technique

There are two types of depth cues by expansion used in the proposed system, which are known as the distance ratio cue and the scale changes cue. In order to observe the behaviour of the distance ratio cue, consider the graph in Figure 3. Figure 3 illustrates four sets of distances from the feature points against the distance of captured image frames. The four sets of distances from the feature points show similar behaviour. However, it is observed that the relationship between the feature points distance and distance from the camera sensor is inversely proportional to each other and closely represent a logarithmic function. Valuable information can be extracted from this relationship, which is a closer object will have a more significant distance changes between feature points (change in the size of the object) compared to an object at a distance.

Figure 3 Distance ratio cue observation (see online version for colours)

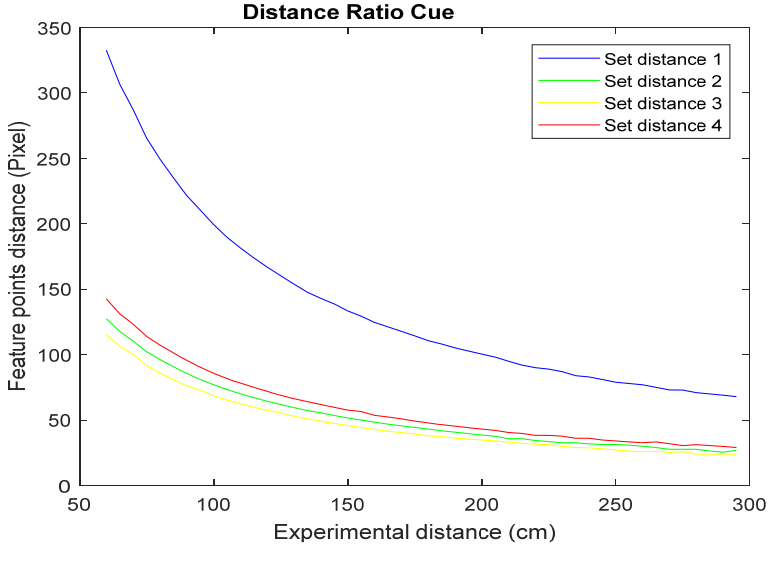

Each of the image frames will generate its own feature points by using the SURF (Bay et al., 2006) technique. The formula for computing distance ratio, dR of the detected feature points is obtained as follows:

$$dR = \frac{D^{If+1}}{D^{If}} \tag{1}$$

where

$$mfp^{If}_{n(i,j)} = \left(L_{x(n)}, L_{y(n)}\right) \tag{2}$$

$$mfp^{If}_{n+1(i,j)} = \left(L_{x(n+1)}, L_{y(n+1)}\right) \tag{3}$$

$$D^{If} = \sqrt{\left(L_{x(n)} - L_{x(n+1)}\right)^2 + \left(L_{y(n)} - L_{y(n+1)}\right)^2} \tag{4}$$

where *mfp* is the matched feature points, L_x and L_y are the location of the pixel in x and y-direction respectively, and *If* represents the image frame where computation is made. The sequence for the matching is conducted as follows, the feature points on image frame 1 will be matched to the feature points on image frame 3 and the feature points on image frame 2 will again be matched to the same feature points on image frame 3 (see Figure 4). The reason why the sequence is fashioned like that is because the image frame 3 will be the final view of the camera sensor towards the surrounding environment.

Figure 4 Matched image frames, (a) image frames 1 (b) image frame 2 (c) image frame 3 (see online version for colours)

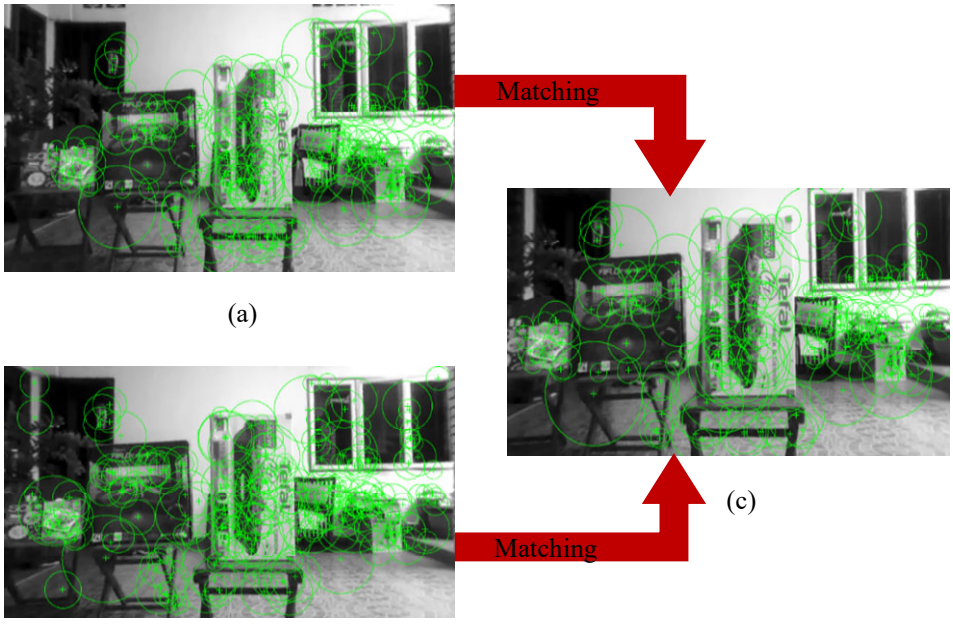

As for scale changes cue, the feature points contain the scale at which the points are being detected. These scale values will respond according to the distance at which the image frame was captured. For example, when similar feature point from the object is detected at a far distance away from the camera sensor, the scale value generated will be practically high compared to the scale value in which the camera sensor is very near to the object (see Table 2). Therefore, the change in scale values of the detected feature points can give rough information about the state position of the object, which is either the object is approaching or moving away from the UAV (camera sensor). It is assumed that if the scale ratio value is less than 1, the matched feature points are incorrect.

Table 2 Scale changes observation

No.	*Image 1*	*Image 2*	*Image 3*	*Ratio Image 3/Image 2*	*Ratio Image 3/Image 1*
1	2.1333	2.8000	4.5333	1.6190	2.1250
2	2.9333	5.4667	11.3333	2.0731	3.8637
3	1.8667	3.0667	5.8667	1.9130	3.1428
4	2.9333	4.8000	10.4000	2.1667	3.5455
5	2.0000	2.8000	5.7333	2.0476	2.8667
6	1.7333	2.8000	5.6000	2.0000	3.2308
7	2.8000	4.4000	8.9333	2.0302	3.1905
8	2.6667	4.0000	8.0000	2.0000	3.0000

3.3 Region classification

As presented earlier, there are two matched image frames that need to be analysed by the proposed system. Each of the matched image frames has different separated distance values (15 cm and 30 cm) from one another. Since the separation distance value is dissimilar, the detection result, particularly the region classification will produce two outputs. Thus, these detection results can be used collectively by making a comparison or deduce the most correct computation for the appearance of obstacles and free region for the safe avoidance path. Table 3 illustrates the full template of distance ratio dR for the respective matched image frames. The image frame can now be categorised into a few regions by using the distance ratio template.

For example, Figure 5(a) shows the distance ratio dR_n^{L15} of 15 cm distance separation derived from the left section of the image frames from one of the detection experiments. Note that observed reference point (ORP) is detected matched feature points in the image frames. If the distance ratio dR_n^{L15} is higher than the reference distance ratio which have been selected 300 cm from the UAV, the detection system will mark the points as an obstacle which represent as logic 1 and vice versa. This process is similar to the thresholding process described in Petrou and Bosdognianni (2010). To be conservative, if the percentage is higher than 40%, the points will be picked as the true feature points on the obstacles.

After the total number of obstacle and non-obstacle feature points has been computed for both the right section and left section of the image frame, zones that are directly portray the safe avoidance path for the UAV can be identified by the following equations:

$$\left(LR_{15}, RR_{15}\right) = \frac{size\left(\hat{mfp}_n^{Lo15}, \hat{mfp}_n^{Ro15}\right)}{size\left(\hat{mfp}_n^{Lf15}, \hat{mfp}_n^{Rf15}\right)} \tag{5}$$

$$Region\ classification = \begin{cases} \left(LR_{15}, RR_{15}\right) > 1, Obstacle\ region \\ \left(LR_{15}, RR_{15}\right) < 1, Free\ region \end{cases} \tag{6}$$

where LR_{15} and RR_{15} refer to the ratio of the left section and right section of the image frame on a 15 cm distance separation. If the ratio is higher than 1, the area of the image frame is considered as the no-flying zone and vice versa. By comparing the ratio from

both sections in the image frame, the proposed detection system is able to initially decide which section in the image frame is the safest for the UAV avoidance action (see Figure 6).

Table 3 Template for distance ratio

Distance (cm)	*Distance ratio dR of 30 cm distance separation*	*Distance ratio dR of 15 cm distance separation*
100	1.45	1.26
150	1.25	1.15
200	1.17	1.11
250	1.14	1.09
300	1.10	1.05
350	1.09	1.04
400	1.07	1.03
450	1.06	1.02
500	1.05	1.01

Figure 5 Thresholding process for region classification (see online version for colours)

ORP 1	ORP 2	ORP 3	ORP 4	ORP 5	ORP 6	ORP 7	ORP 8	ORP 9	ORP 10
0	1.056	1.085	1.093	1.143	1.008	1.080	1.107	1.107	1.130
1.056	0	1.081	1.077	1.094	1.012	1.064	1.083	1.084	1.074
1.085	1.081	0	0.927	1.051	1.006	1.073	1.056	1.063	1.080
1.093	1.077	0.927	0	1.071	0.990	1.085	1.081	1.080	1.092
1.143	1.094	1.051	1.071	0	1.017	1.162	1.066	1.068	1.152
1.008	1.012	1.006	0.990	1.017	0	1.012	0.998	0.996	1.012
1.080	1.064	1.073	1.085	1.162	1.012	0	1.087	1.082	1.013
1.107	1.083	1.056	1.081	1.066	0.998	1.087	0	1.067	1.103
1.107	1.084	1.063	1.080	1.068	0.996	1.082	1.067	0	1.101
1.13	1.074	1.080	1.092	1.152	1.012	1.013	1.103	1.101	0

(a)

ORP 1	ORP 2	ORP 3	ORP 4	ORP 5	ORP 6	ORP 7	ORP 8	ORP 9	ORP 10
0	1	1	1	1	0	1	1	1	1
1	0	1	1	1	0	1	1	1	1
1	1	0	0	1	0	1	1	1	1
1	1	0	0	1	0	1	1	1	1
1	1	1	1	0	0	1	1	1	1
0	0	0	0	0	0	0	0	0	0
1	1	1	1	0	0	0	1	1	0
1	1	1	1	1	0	1	0	1	1
1	1	1	1	1	0	1	1	0	1
1	1	1	1	1	0	0	1	1	0
89%	*89%*	*78%*	*78%*	*78%*	*0%*	*78%*	*89%*	*89%*	*78%*

Flow

(b)

If both sections of the image frame (left and right) have a ratio higher than 1, the fixed reference distance ratio (1.05 for 15 cm and 1.10 for 30 cm) will be changed gradually to a certain value that will uncover the true identify of both sections. If one of the side section changes first its ratio value from greater than 1 to lower than 1, it is safe to assume that the side section will provide less resistance to the UAV (see Figure 7). This technique is also applied when both sections have a ratio lower than 1. The whole region detection process described above will be repeated on the matched image frames having 30 cm distance separation. When the side sections on both matched image frames are similar in terms of the region categorisation, the confidence level for the accuracy of the detected regions, be it an obstacle region or free region, will certainly be high. For example, if the right section on both matched image frames (15 cm and 30 cm distance

separation) consists of the free region, then, the proposed system will consider the right section of the image frames as the ultimate free region (safe path) for the UAV.

Figure 6 Classification of true obstacle region and free region in the image frame (see online version for colours)

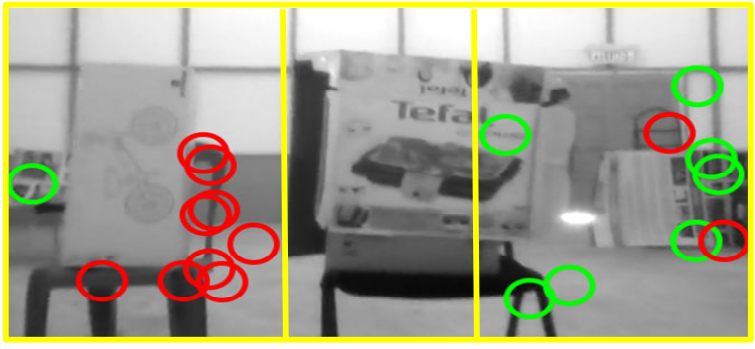

Figure 7 Uncover true identity of the area by changing the reference distance ratio, (a) reference distance ratio = 1.05 (b) reference distance ratio = 1.06 (c) reference distance ratio = 1.07 (see online version for colours)

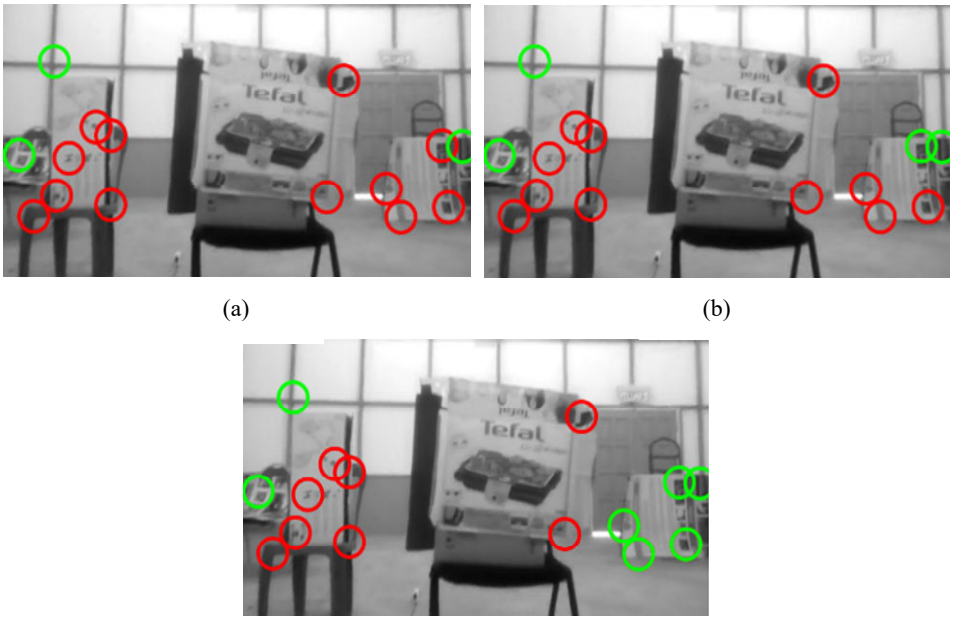

(a) (b)

(c)

Since the confidence level in this situation is high, the feature points on both matched image frames will be combined to extend the volume of the detected region especially the free region as shown in Figure 8. If the identity of side sections on both matched image frames are not similar, the result from the 30 cm distance matched image frames will be selected.

Figure 8 Free region feature points combination, (a) feature points in 15 cm matched image frame (b) feature points in 30 cm matched image frame (c) combination of feature points from both of matched image frames (see online version for colours)

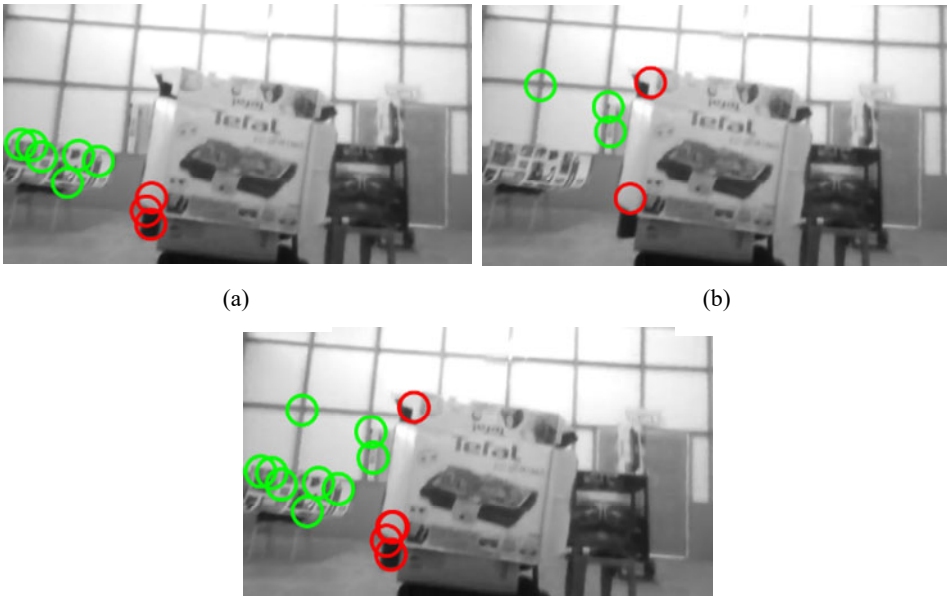

(a) (b)

(c)

3.4 Safe avoidance path identification

Once the free region has been identified, the exact path for the safe avoidance action must be extracted. When the section of the image frame contains the free region feature point but none for obstacle region feature points, the proposed system will divide the free region feature into several groups by K-mean clustering (Likas et al., 2003). Next, the proposed system will select the denser cluster as the safe avoidance path (see Figure 9). If clustering is not performed, it might cause complication for the UAV to avoid the obstacles. For example, if the texture-less obstacles are situated within the perimeter of the free region feature points (without clustering), then, the proposed system will assume that the whole path is safe and free from any obstacles.

Figure 9 Cluster the free region feature points, (a) computed free region feature points (b) free region feature points clustering (see online version for colours)

(a) (b)

On the other hand, when the section of the image frame contains the mixture of free region and obstacle region feature points. The convex hull algorithm is used to isolate the obstacle region feature points from the free region feature points (Greenfield, 1990). Once the convex hull (Cv_S, Cv_M) is established, the next step is to find the free region feature points within this hull according to the situations stated in Table 4. Note that, (Ffp_n^{SI}, Ffp_n^{MI}) and (Ofp_n^S, Ofp_n^M) refers to free region points inside the convex hull and obstacle region feature points, respectively. Superscripts S and M refers to, side and middle section of the image frames, respectively.

Table 4 Application of convex hull

Situation	*Result*
$(Ffp_n^{SI}, Ffp_n^{MI}) > (Ofp_n^S, Ofp_n^M)$	Consider convex hull as part of the free region (obstacle feature points are falsely calculated).
$(Ffp_n^{SI}, Ffp_n^{MI}) < (Ofp_n^S, Ofp_n^M)$	Consider convex hull as part of the obstacle region. The (Ffp_n^{SI}, Ffp_n^{MI}) will be excluded (see Figure 11).

Figure 10 Isolation technique for the detected feature points, (a) convex hull is formed from the obstacle region feature points (b) the free region feature point inside the convex hull is removed (see online version for colours)

(a) (b)

4 Implementation and experimental setup

The platform used in the experimentation is the AR Drone 2.0 elite edition, a low-cost UAV built by the company Parrot. This UAV was selected because it is a low-cost small commercial UAV available in the market and also has stable flying properties. Camera sensors used is the built-in UAV camera with 1,280 × 720 resolution and horizontal field of view (FOV) is 62 degrees. However, we use a lower resolution (640 × 360) to increase the computation speed of the algorithm.

For range sensors, LIDAR Lite v3 is selected. It is selected because the measured range is very accurate and high as compared to other sensors like infrared and ultrasonic sensors. Also, it is considered low-cost and small in sizes when compare with other wide scanning LIDAR. Arduino Nano v3.0 ATMEGA328 is used to read and connect LIDAR sensor to the system (see Figure 11). In this research, the primary tool or software that we used for analysis and calculation is MATLAB 2017a. The software contains a computer

vision system toolbox which makes it possible to use as tool development for our obstacle detection and avoidance system. Our entire algorithm processed on a ground laptop which is quad-core Intel i7 running Windows operating system. Communication and data transfer between UAV including LIDAR sensor and ground laptop are done by XBee radio module. The radio frequency (RF) data rate of this module was up to 250,000 bps and operates at frequency 2.4 Ghz (Fajriansyah et al., 2018).

Figure 11 UAV platform configuration, (a) AR Drone 2.0 (b) LIDAR Lite v3 (c) camera sensor (d) Arduino Nano (e) Xbee Pro S1 (see online version for colours)

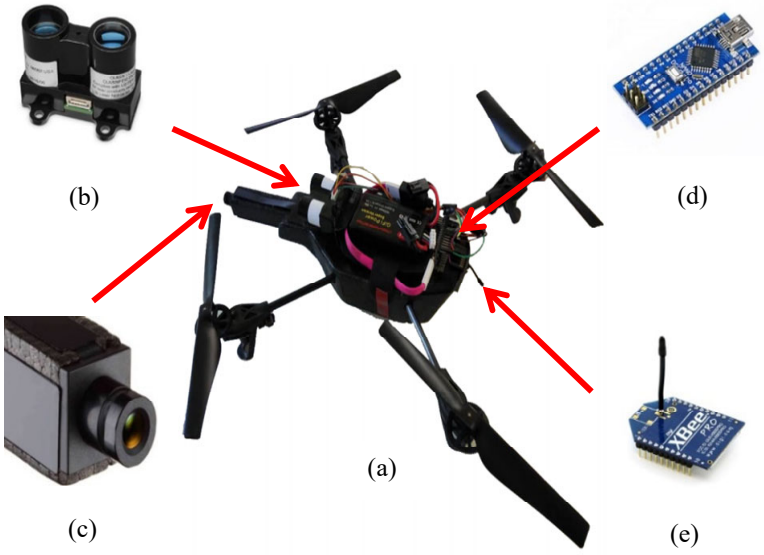

Figure 12 Obstacles used in the experiment, (a) obstacle 1 (good texture) (b) obstacle 2 (good texture) (c) obstacle 3 (poor texture) (d) obstacle 4 (texture-less) (see online version for colours)

In order to evaluate the performance and capability of the proposed system, a number of obstacle detection and avoidance experiments with different kinds of situations introduced in the operating environment have been carried out. All of the experiments are performed in an indoor environment inside one of the rooms in the aircraft's hangar. The size of the room is 10 m in length and 9.8 m in width. All of the algorithm processes and computations will be carried out by the external ground station (Intel i7-2670QM

processor) with the help of Software Development Kit V.1.1. The external software selected for the video streaming channel from the UAV are the FFmpeg and ManyCam. The obstacles used in the experiments are shown in Figure 12 and note that these introduced obstacles vary in sizes and textures.

Figure 13 Situation in the performed experiment where the (a) yellow box, (b) black box and (c) red box (c) represent the frontal obstacle, side obstacle and fixed obstacle, respectively (see online version for colours)

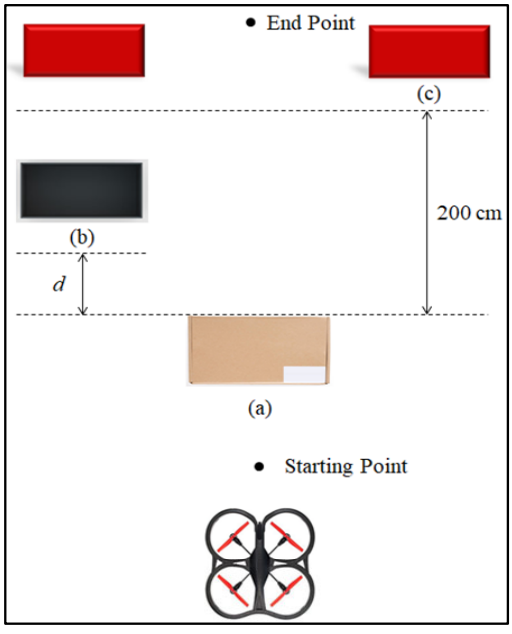

Note: *d* is the distance between frontal obstacle and side obstacle.

The UAV will fly straight into the operating environment from the starting point to the endpoint and the obstacles will be placed between these points. There are three types of obstacle used in the experiment namely frontal, side and fixed obstacles. In the preliminary experiments, only frontal obstacle is placed in the operating environment. After finished with the preliminary experiments, the side obstacle will be introduced alongside the frontal obstacle. The distance of the side obstacle from the frontal obstacle will be increased gradually as illustrated in Figure 13. On top of that, the side obstacle is switched from the right to the left of the frontal obstacle to ensure that the proposed system is able to recognise the right safe avoidance path even though the operating environment situation is rapidly changed.

5 Result and discussion

As seen from the results (see Figure 14), no failures can be observed on each of the single stationary obstacles cases. The UAV successfully executed the mission from the beginning to the end without crashing into one of the introduced obstacles specifically the frontal obstacle. The avoidance path taken by the UAV on each test is different is due to

the feature detection of the free region in the image frame is different. As a result, the safe avoidance path which is derived from the available free region of the image frame will also be different.

In the situation where the side obstacle is introduced, only obstacle 1, obstacle 3 and obstacle 4 are used as the side obstacle in the multiple obstacle situation (see Figure 15–Figure 17). The blue box represents the side obstacle that is placed right next to the frontal obstacle. The proposed system successfully guided the UAV into the correct avoidance path in the operating environment towards the goal.

Figure 14 Result of the avoidance path for single obstacle situation, (a) single obstacle Case 1 (b) single obstacle Case 2 (c) single obstacle Case 3 (d) single obstacle Case 4 (see online version for colours)

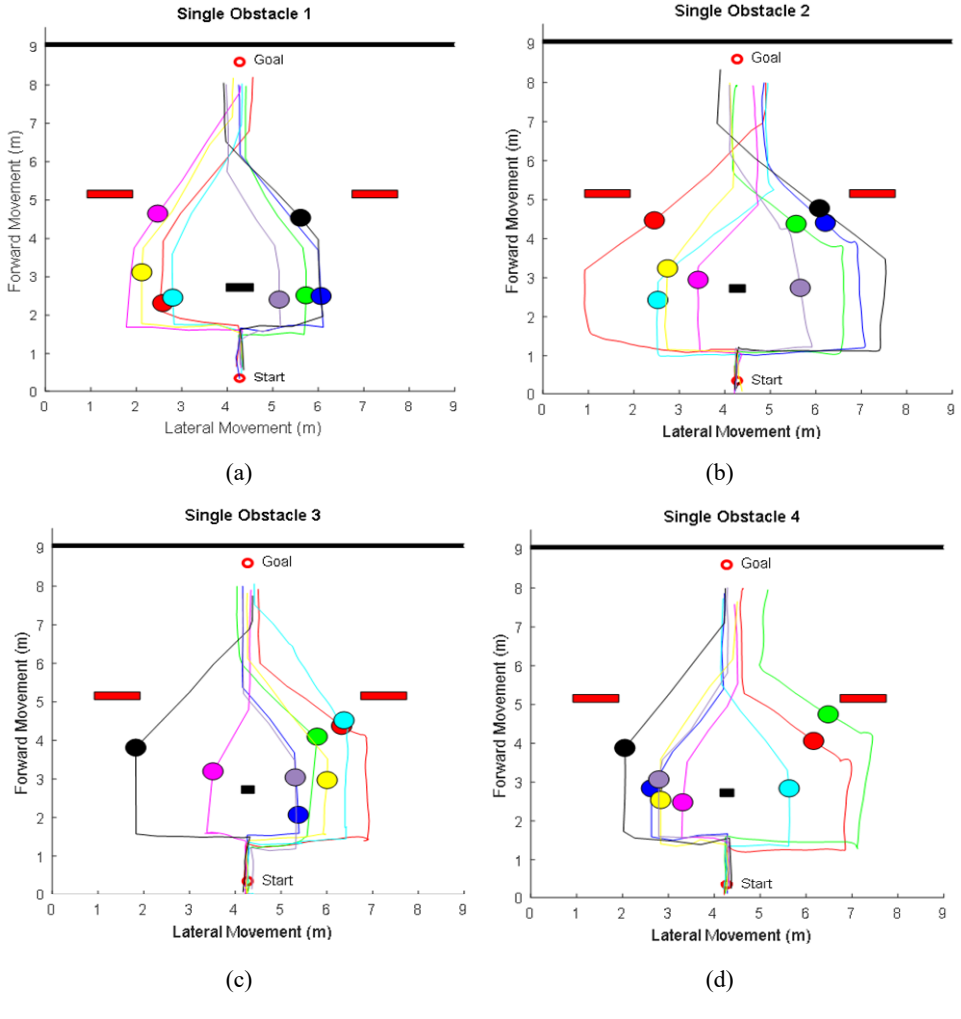

Note: Black box represents frontal obstacle and red boxes represent fixed obstacles.

Figure 15 Result of the avoidance path for multiple obstacle situation with aligned side obstacle, (a) side obstacle Case 1 (b) side obstacle Case 3 (c) side obstacle Case 4 (see online version for colours)

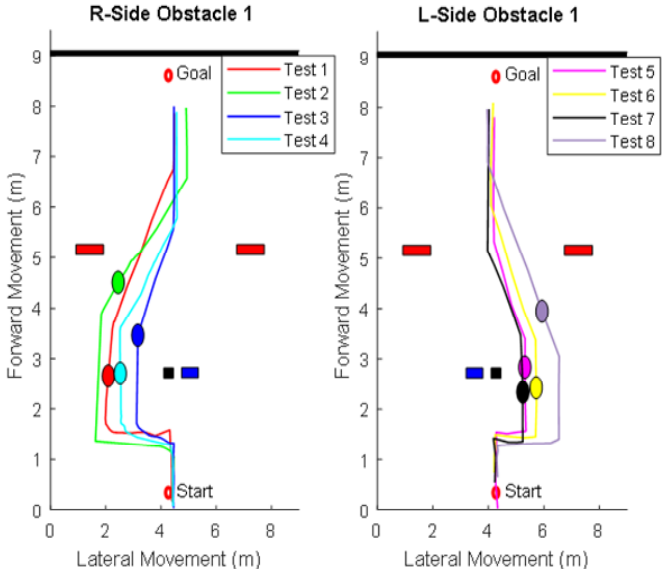

(a)

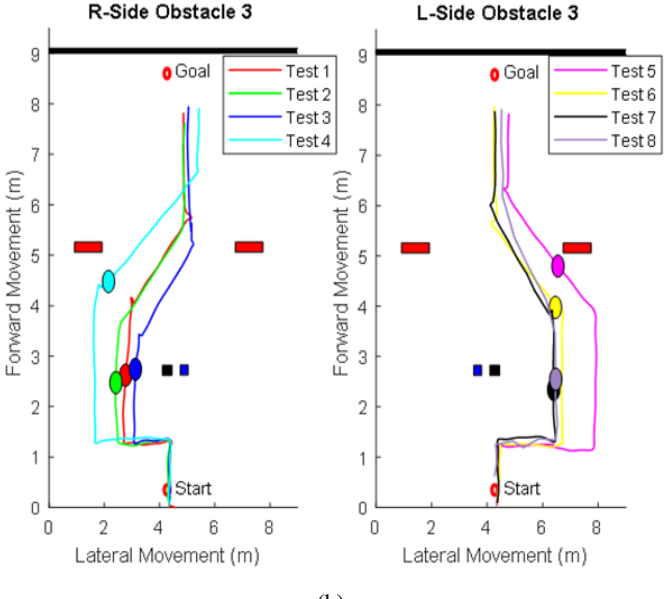

(b)

Figure 15 Result of the avoidance path for multiple obstacle situation with aligned side obstacle, (a) side obstacle Case 1 (b) side obstacle Case 3 (c) side obstacle Case 4 (continued) (see online version for colours)

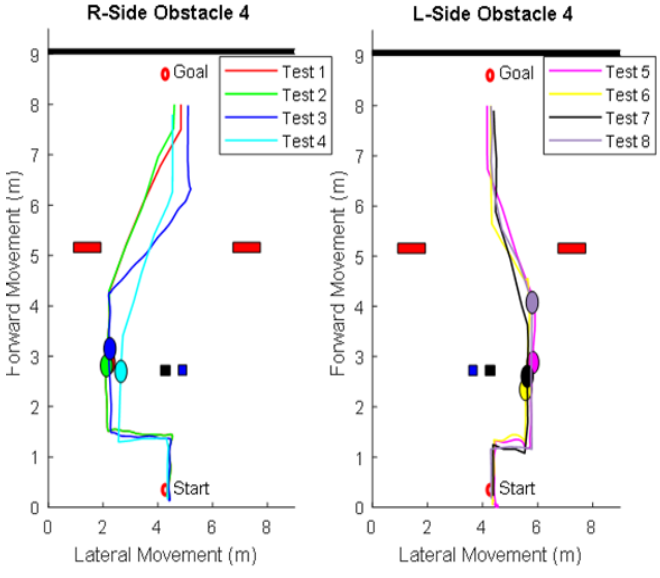

(c)

Figure 16 Result of the avoidance path for multiple obstacles situation with side obstacle located 60 cm away from the frontal obstacle, (a) side obstacle Case 1 (b) side obstacle Case 3 (c) side obstacle Case 4 (see online version for colours)

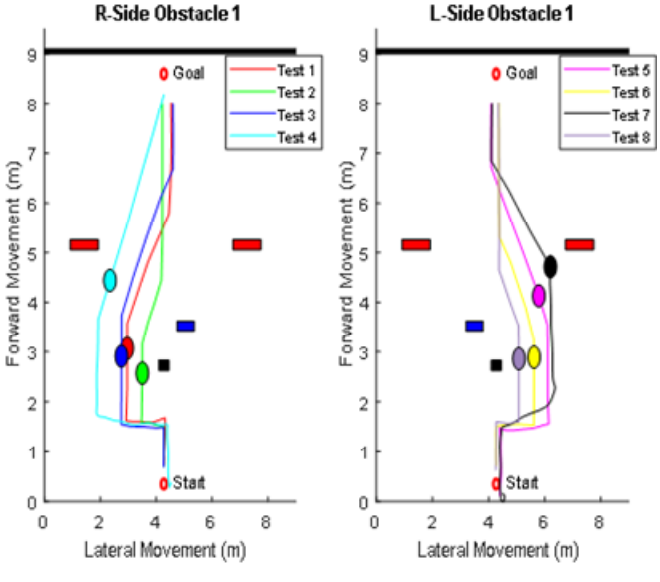

(a)

Figure 16 Result of the avoidance path for multiple obstacles situation with side obstacle located 60 cm away from the frontal obstacle, (a) side obstacle Case 1 (b) side obstacle Case 3 (c) side obstacle Case 4 (continued) (see online version for colours)

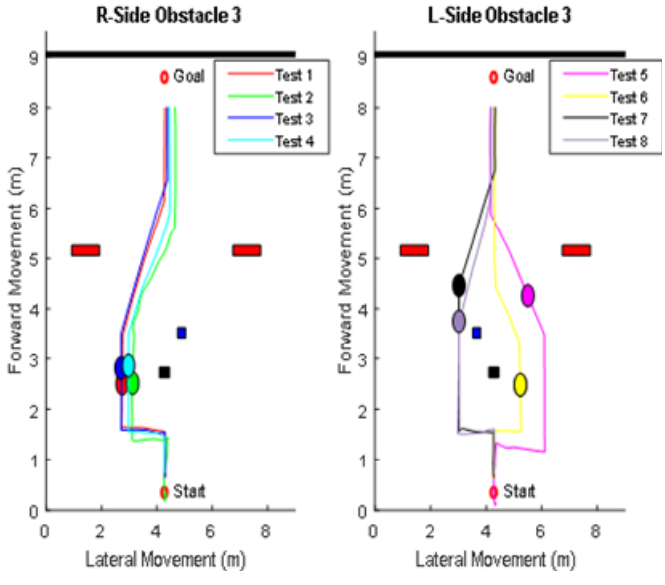

(b)

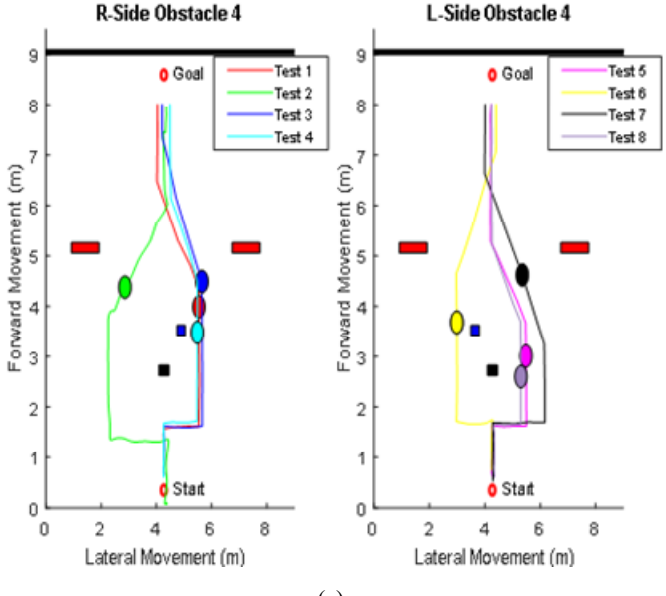

(c)

Figure 17 Result of the avoidance path for multiple obstacles situation with side obstacle located 120 cm away from the frontal obstacle, (a) side obstacle Case 1 (b) side obstacle Case 3 (c) side obstacle Case 4 (see online version for colours)

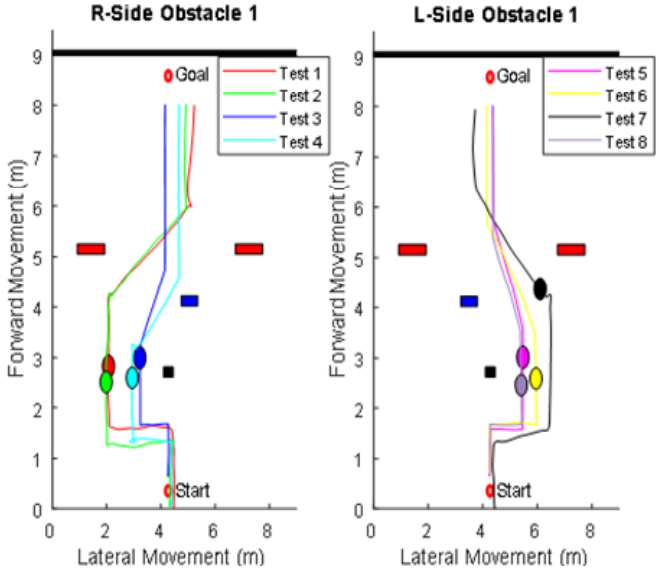

(a)

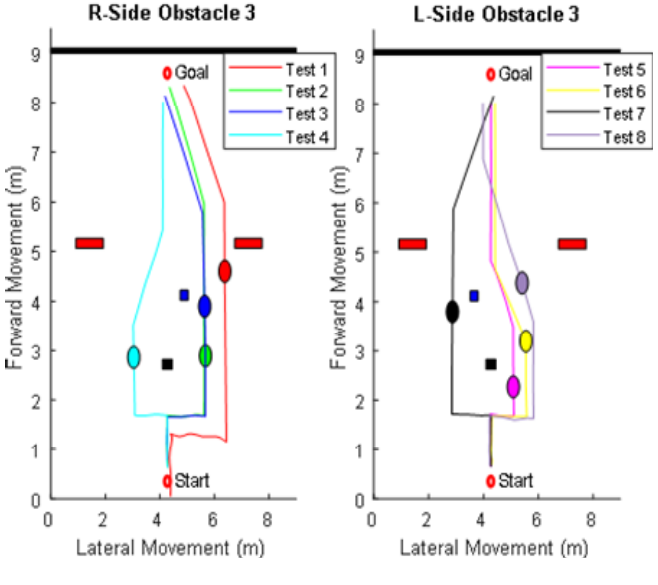

(b)

Figure 17 Result of the avoidance path for multiple obstacles situation with side obstacle located 120 cm away from the frontal obstacle, (a) side obstacle Case 1 (b) side obstacle Case 3 (c) side obstacle Case 4 (continued) (see online version for colours)

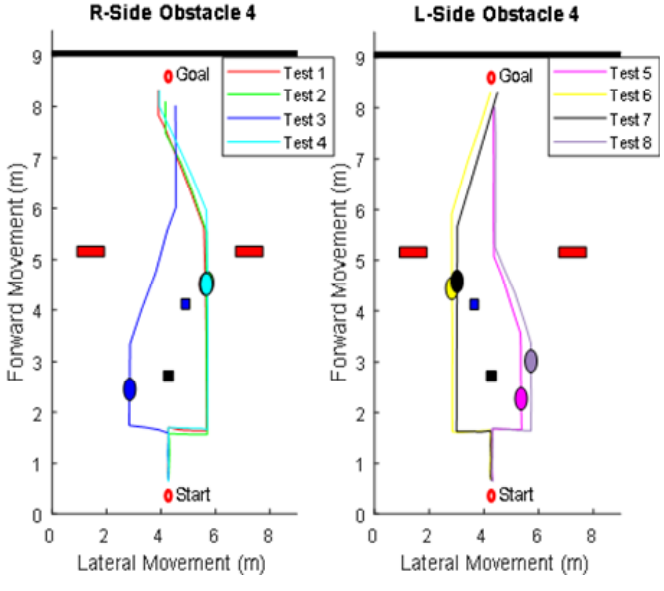

(c)

On top of that, the proposed system was able to recognise the appearance of the side obstacle including texture-less obstacle, which includes its position and location in the UAV operating environment. This is true for a situation when the side obstacle is aligned with frontal obstacle (see Figure 15). As can be observed, in each position of the side obstacle either left or right for all of the aligned side obstacle cases, the proposed obstacle detection and avoidance system was able to create a safe avoidance path on the opposite side of the introduced side obstacle. Even though the side obstacle 4 is texture-less obstacle, the proposed obstacle detection and avoidance system was still able to create the perfect safe avoidance path for the UAV avoidance action.

There is a noticeable difference between the situations when the side obstacle is aligned with frontal obstacle and when the side obstacle is far away from the frontal obstacle, which the direction of the safe avoidance path [see Figures 16(b), 16(c), 17(b) and 17(c)]. As seen from the result especially the side obstacle Cases 3 and 4 (60 cm or 120 cm away from the frontal obstacle), there are few avoidance paths that are created on the same side as the introduced side obstacle, which is not a preferred direction of the avoidance path. Even though some of the avoidance path is considered close to the obstacle (e.g., Test 1 and Test 4 of side obstacle Case 4 for 60 cm), the avoidance path is still safe because the path itself is derived from the detected free region available in the operating environment. Since side obstacle 1 contains very high and clear texture, it is easy for the proposed system to detect the appearance of the obstacle even though it is placed far away (60 cm or 120 cm) from the frontal obstacle, which is approximately about 210–270 cm from the location of the UAV when the UAV platform encountered the first obstacle (frontal obstacle).

As for the side obstacle 3, it has a poor texture due to the distance from the UAV. As a result, some of the tests show that the proposed system unable to detect the appearance of the obstacle. This also true for the situations where the side obstacle 4 is introduced. Even though the avoidance path is on the same side as the side obstacle, the proposed system was still able to recognise and identify the ultimate free region of the operating environment from the captured image frames. Based on the result, it is important to highlight that, since the proposed system able to recognise the free region and obstacle region in the environment, the detection system solved the main problem encountered by the vision-based obstacle detection on avoiding the obstacle that contains poor texture in its surface or texture-less obstacle, which is aligned with the contribution of the research.

The limitation of the proposed obstacle detection system comes from streaming the live video from the camera sensor. Streaming live video from the camera sensor suffers from the streaming latency of about 400 ms. Due to this streaming latency, the UAV platform cannot move too rapidly in the operating environment for the detection of the obstacles. If the UAV moves excessively fast, the image frame sequence captured by the camera sensor, which is image 1, image 2 and image 3 will be incorrect. It is because the captured distance of that particular image frame from the UAV is not closely similar to the actual reference distance (see Figure 2). As a consequence, the UAV will have to fly slower to reduce the effect of the streaming latency.

6 Conclusions

This paper presents research work on the obstacle detection and avoidance system for the UAV. The aim of this research project is to develop a robust autonomous obstacle detection and avoidance system for small-sized UAV using multiple and different sensor-based integrations. Previous works on this field are bounded by the major constraints of the UAV platform, which is the payload capacity and physical size constraints. There are two types of obstacle detection-based, which is vision-based sensor and range-based sensor. These two obstacle detection-based types have their own advantages and disadvantages. Due to the mentioned constraints, most of the previous obstacle detection and avoidance system will only consist of one obstacle detection-based. The proposed system solved these obstacle detection difficulties by merging both sensor-based together into a single obstacle detection system. The LIDAR Lite v3, which is the range sensor, will act as the secondary detection sensor that measures the distance value of the obstacle and also initiate the detection process performed by the primary detection sensor, which is the camera sensor. Cues from expansion of the features points are used to extract the depth information of the environment and classify the region. These regions represent the actual environment situation that the UAV faced. From these regions, the proposed system will create the safe avoidance path for the UAV. The depth perception technique in this paper (distance ratio cue and scale changes cue) is based on the expansion of the detected features points between the image frames.

The results show that the texture appearance of the obstacle will not affect the judgement of the proposed system to create the safe avoidance path for the UAV. Other than the ability to only detect the frontal obstacle, the proposed system will access and observed the operating environment as a whole before deciding on the safe avoidance path. The conclusion that can be drawn from the experiment is the detection of the

obstacle appearance depends on the perspective of the camera sensor. If the obstacle is very far from the UAV but has a clear appearance in terms of the texture from the view of the camera sensor, then the proposed system will be able to produce the safe avoidance path in a preferred direction. The proposed system will generate the feature points from the operating environment and classify the regions in the operating environment according to these feature points. Therefore, if the obstacle (obstacle region feature points) cannot be detected due to texture appearance of the obstacle, the proposed obstacle detection and avoidance still has the free region feature points to generate the safe avoidance path for the UAV. On the other hand, if the obstacles are detected during the detection computation processes, safe avoidance path will be safely created on the opposite side of the obstacle to be conservative. Besides, the safe avoidance path created will still follow the free region feature points detected unlike the tolerance extension from the previous obstacle detection and avoidance systems (Al-Kaff, 2017; Aguilar et al., 2017; Mori and Se, 2013). The proposed system is able to create the safe avoidance path even when the distance side obstacle is about 270 cm from the UAV. This distance is twice the distance of the frontal obstacle detection by a prior research work (Al-Kaff et al., 2017).

One of the recommendations for future work is to use higher degree camera sensor for better coverage FOV. If the angle coverage of the FOV is high, more areas or regions in the operating environment can be detected. As a result, there will be more free regions in the image frame that can be selected as the safe avoidance path region for the UAV. Finally, it is desirable to work with data especially the data derived from the distance ratio cues to predict or observe the environment. If the distance ratio cues data is trained to certain degrees, it can be used to build a real-time depth map of the operating environment which favourable to both navigation system and obstacle detection system.

Acknowledgements

The research was supported by the University Tun Hussein Onn Malaysia (UTHM) through Tier 1 (H920).

References

Aguilar, W., Casaliglla, V. and Pólit, J. (2017) 'Obstacle avoidance based-visual navigation for micro aerial vehicles', *Electronics*, Vol. 6, No. 1, p.10, DOI: 10.3390/electronics6010010.

Al-Kaff, A. et al. (2017) 'Obstacle detection and avoidance system based on monocular camera and size expansion algorithm for UAVs', *Sensors (Switzerland)*, Vol. 17, No. 5, p.1061, DOI: 10.3390/s17051061.

Al-Kaff, A.H. (2017) *Vision-Based Navigation System for Unmanned Aerial Vehicles*, PhD thesis, Universidad Carlos III De Madrid, Madrid.

Bachrach, A., He, R. and Roy, N. (2009) 'Autonomous flight in unknown indoor environments', *International Journal of Micro Air Vehicles*, Vol. 1, No. 4, pp.217–228, DOI: 10.1260/175682909790291492.

Bay, H., Tuytelaars, T. and Van Gool, L. (2006) 'SURF: speeded up robust features', in *European Conference on Computer Vision*, pp.404–417, DOI: 10.1007/11744023_32.

Bills, C., Chen, J. and Saxena, A. (2011) 'Autonomous MAV flight in indoor environments using single image perspective cues', *IEEE International Conference on Robotics and Automation*, pp.5776–5783.

Carrio, A. et al. (2020) 'Onboard detection and localization of drones using depth maps', *IEEE Access*, Vol. 8, pp.30480–30490, DOI: 10.1109/ACCESS.2020.2971938.

De Croon, G.C.H.E. et al. (2011) 'The appearance variation cue for obstacle avoidance', *IEEE Transactions on Robotics*, Vol. 28, No. 2, pp.529–534.

Deng, C. et al. (2014) 'Unmanned aerial vehicles for power line inspection: a cooperative way in platforms and communications', *Journal of Communications*, Vol. 9, No. 9, pp.687–692, DOI: 10.12720/jcm.9.9.687-692.

Erdos, D., Erdos, A. and Watkins, S.E. (2013) 'An experimental UAV system for search and rescue challenge', *IEEE Aerospace and Electronic Systems Magazine*, Vol. 28, No. 5, pp.32–37, DOI: 10.1109/MAES.2013.6516147.

Eschmann, C., Kuo, C-M. and Boller, C. (2012) 'Unmanned aircraft systems for remote building inspection and monitoring', *Proceedings of the 6th European Workshop on Structural Health Monitoring*, Vol. 2, pp.1–8.

Fajriansyah, B., Ichwan, M. and Susana, R. (2018) 'Evaluasi Karakteristik XBee Pro dan nRF24L01+ sebagai Transceiver Nirkabel', *ELKOMIKA: Jurnal Teknik Energi Elektrik, Teknik Telekomunikasi, & Teknik Elektronika*, Vol. 4, No. 1, p.83, DOI: 10.26760/elkomika.v4i1.83.

Greenfield, J.S. (1990) *A Proof for a QuickHull Algorithm*, Electrical Engineering and Computer Science – Technical Reports No. 65, Syracuse University, New York.

Kim, J. et al. (2014) 'Collision avoidance system for agricultural unmanned helicopter using LIDAR sensor', in *Asia-Pacific International Symposium on Aerospace Technology*.

Leong, W.L. et al. (2021) 'Vision-based sense and avoid with monocular vision and real-time object detection for UAVs', *2021 International Conference on Unmanned Aircraft Systems, ICUAS 2021*, pp.1345–1354, DOI: 10.1109/ICUAS51884.2021.9476746.

Likas, A., Vlassis, N. and Verbeek, J. (2003) 'The global k-means clustering algorithm', *Pattern Recognition*, Vol. 36, No. 2, pp.451–461.

Majumder, S., Shankar, R. and Prasad, M.S. (2015) 'Obstacle size and proximity detection using stereo images for agile aerial robots', *2nd International Conference on Signal Processing and Integrated Networks, SPIN 2015*, pp.437–442, DOI: 10.1109/SPIN.2015.7095261.

Mori, T. and Scherer, S. (2013) 'First results in detecting and avoiding frontal obstacles from a monocular camera for micro unmanned aerial vehicles', *Proceedings – IEEE International Conference on Robotics and Automation*, pp.1750–1757, DOI: 10.1109/ICRA.2013.6630807.

Mori, T. and Se, S. (2013) 'First results in detecting and avoiding frontal obstacle from monocular camera for micro unmanned aerial vehicles', *2013 IEEE International Conference on Robotics and Automation (ICRA)*, Vol. 53, No. 9, pp.1689–1699, DOI: 10.1017/CBO9781107415324.004.

Nhair, R.R. and Al-Assadi, T.A. (2020) 'Vision-based obstacle avoidance for small drone using monocular camera', *IOP Conference Series: Materials Science and Engineering*, Vol. 928, No. 3, DOI: 10.1088/1757-899X/928/3/032048.

Payal, Akashdeep and Singh, C.R. (2020) 'A summarization of collision avoidance techniques for autonomous navigation of UAV', in *International Conference on Unmanned Aerial System in Geomatics*, pp.393–401, DOI: 10.1007/978-3-030-37393-1_23.

Petrou, M. and Bosdognianni, P. (2010) *Image Processing: The Fundamentals*, John Wiley & Sons Ltd., Chichester.

Rudol, P. and Doherty, P. (2008) 'Human body detection and geolocalization for UAV search and rescue missions using color and thermal imagery', in *IEEE Aerospace Conference*, pp.1–8.

Scherer, J. et al. (2015) 'An autonomous multi-UAV system for search and rescue', *Proceedings of the First Workshop on Micro Aerial Vehicle Networks, Systems, and Applications for Civilian Use – DroNet '15*, pp.33–38, DOI: 10.1145/2750675.2750683.

She, X. et al. (2021) 'Multi-obstacle detection based on monocular vision for UAV', *Proceedings of the 16th IEEE Conference on Industrial Electronics and Applications, ICIEA 2021*, pp.1067–1072, DOI: 10.1109/ICIEA51954.2021.9516384.

Torrero, L. et al. (2014) 'The use of micro-UAV to monitor active landslide scenarios', in *Engineering Geology for Society and Territory – Volume 5*, pp.701–704, DOI: 10.1007/978-3-319-09048-1.

Whalley, M. et al. (2009) 'Field-testing of a helicopter UAV obstacle field navigation and landing system', in *65th Annual Forum of the American Helicopter Society*, Grapevine, TX [online] http://armyscienceconference.com/manuscripts/E/EP-008.pdf.

Yoo, D., Won, D. and Tahk, M. (2011) 'Optical flow based collision avoidance of multi-rotor UAVs in urban environments', *International Journal of Aeronautical and Space Sciences*, Vol. 12, No. 3, pp.252–259, DOI: 10.5139/IJASS.2011.12.3.252.

Zufferey, J.C. and Floreano, D. (2006) 'Fly-inspired visual steering of an ultralight indoor aircraft', *IEEE Transactions on Robotics*, Vol. 22, No. 1, pp.137–146, DOI: 10.1109/TRO.2005.858857.